AIAA Guidance, Navigation, and Control Conference and Exhibit
16 - 19 August 2004, Providence, Rhode Island

AIAA 2004-5335

Feasible Flight Paths for Cooperative Generation of a Phantom Radar Track

Keith B. Purvis*
University of California, Santa Barbara, CA 93106–5070, U.S.

Phillip R. Chandler†
Air Force Research Laboratory, Wright-Patterson AFB, OH 45433–7531, U.S.

Meir Pachter‡
Air Force Institute of Technology, Wright-Patterson AFB, OH 45433–7765, U.S.

Electronic attack on air defense radar networks by a team of Electronic Combat Air Vehicles (ECAVs) is explored. The scope of the attack considered is the creation of a coherent phantom track in two dimensions—range and azimuth—by a team of cooperatively controlled ECAVs, where each ECAV is capable of intercepting and sending delayed returns of radar pulses. Severe restrictions are shown when a constant-speed ECAV and constant-speed phantom track are assumed. Dynamic limitations on an ECAV are presented mathematically and through simulation for straight and circular phantom tracks and specified ranges on the phantom target speed, ECAV speed, and ECAV region of antenna operation. Based on results for a straight or circular phantom track, generalized bounds for the initial conditions and time-dependent flyable ranges of a team of ECAVs are presented. These bounds are then used with coordination functions to formulate a decentralized cooperative control problem for the scenario of three radars versus three ECAVs generating a straight phantom track.

Nomenclature

$\mathcal{B}$	Space where placement of a phantom track is possible for all radar/ECAV pairs
$\mathcal{T}_{\mathcal{B}}$	Set of all phantom track functions $f(x)$ possible for ECAV team to generate
a	Horizontal distance from center of circular phantom track to radar
a_E	ECAV acceleration—time derivative of velocity
b	Vertical distance from center of circular phantom track to radar
c	Speed of light
$circle$	2-D Circular boundary of radius R_{max} inside which radar can operate and see targets
$cone$	2-D Wedge-shaped boundary inside which ECAV antennas can deceive radar
E	ECAV
f	Phantom track function of x that ECAV team could generate for radar network
h	Coordination function providing individual ECAV's cost versus different phantom tracks
h_E	ECAV heading angle—absolute
h_r	Function that determines valid initial conditions and flyable ranges for ECAV
$h_{\mathcal{T}}$	Function that maps parameters to all possible phantom tracks for ECAV team
I	Ordered set of index numbers
$icost$	ECAV's cost to move to its initial position required for a given phantom track

*Graduate Student Researcher, Department of Mechanical and Environmental Engineering, Engineering II Bldg. Room 2355, Santa Barbara, CA 93106–5070, Student Member AIAA.
†Senior Control Systems Engineer, AFRL/VACA, 2210 8th Street, WPAFB, OH 45433–7531, Member AIAA.
‡Professor, Department of Electrical and Computer Engineering, 2950 P Street, Bldg. 640 Room 224, WPAFB, OH 45433–7765, Member AIAA.

Report Documentation Page

Form Approved
OMB No. 0704-0188

1. REPORT DATE	2. REPORT TYPE	3. DATES COVERED
AUG 2004		**00-00-2004 to 00-00-2004**

4. TITLE AND SUBTITLE	5a. CONTRACT NUMBER
Feasible Flight Paths for Cooperative Generation of a Phantom Radar Track	5b. GRANT NUMBER
	5c. PROGRAM ELEMENT NUMBER
6. AUTHOR(S)	5d. PROJECT NUMBER
	5e. TASK NUMBER
	5f. WORK UNIT NUMBER
7. PERFORMING ORGANIZATION NAME(S) AND ADDRESS(ES) **Air Force Research Laboratory,Air Vehicles Directorate,Wright Patterson AFB,OH,45433**	8. PERFORMING ORGANIZATION REPORT NUMBER
9. SPONSORING/MONITORING AGENCY NAME(S) AND ADDRESS(ES)	10. SPONSOR/MONITOR'S ACRONYM(S)
	11. SPONSOR/MONITOR'S REPORT NUMBER(S)

12. DISTRIBUTION/AVAILABILITY STATEMENT
Approved for public release; distribution unlimited

13. SUPPLEMENTARY NOTES
The original document contains color images.

14. ABSTRACT

15. SUBJECT TERMS

16. SECURITY CLASSIFICATION OF:			17. LIMITATION OF ABSTRACT	18. NUMBER OF PAGES	19a. NAME OF RESPONSIBLE PERSON
a. REPORT	b. ABSTRACT	c. THIS PAGE			
unclassified	**unclassified**	**unclassified**		**20**	

n	Number of radars in a given scenario
R	Phantom target range from radar
r	ECAV range from radar
R_{max}	Maximum operational range of radar
rd	Location of radar in x and y coordinates
s	Switching function/indicator
T	Phantom target
t	Time
t_d	Time delay for ECAV to hold radar pulse
t_s	Switching time
$tcost$	ECAV's cost over time to generate a given phantom track
x	Horizontal coordinate in 2-D space
y	Vertical coordinate in 2-D space
ECAV	Electronic Combat Air Vehicle
LOS	Line of sight from radar to ECAV/phantom target
PRF	Pulse repetition frequency

Subscripts

0	Value at the initial time
c	Variable set constant
i	Index number for radar/ECAV pairs
j	Index number
m	Nominal or average
$psmax$	Pseudo-maximum
$psmin$	Pseudo-minimum
x	x-component of variable—horizontal
y	y-component of variable—vertical

Symbols

α	Ratio of phantom target speed to ECAV speed
β	Absolute heading of phantom track—independent of radar/ECAV pair
χ	Angle between current LOS and line from center of circular phantom track to radar
ϕ_E	ECAV course—relative to θ
ϕ_T	Phantom target course—relative to θ
ψ	Angle between initial LOS and phantom target heading
ρ	Radius of circular phantom track
$\bar{\theta}$	Constant angle from 0 degrees heading to initial LOS
θ	ECAV/phantom target bearing from radar
v_E	ECAV speed
v_T	Phantom target speed
ξ	Heading angle from center of circular phantom track to radar

Superscripts

0	Solved forward in time using initial values
A	Solution corresponding to ECAV system A
f	Solved backward in time using final values

I. Introduction

This paper focuses on using unmanned Electronic Combat Air Vehicles (ECAVs) to cooperatively deceive a radar network by creating a coherent phantom track, which allows the network to detect and track the motion of an air vehicle that does not actually exist. A radar network is defined as a geometric arrangement (possibly changing with time) of two or more radars, which are able to communicate with each other; hence, multiple radars may be used to track and correlate the same target. Ref. 1 provides a thorough background on radars and how they work. For this paper, generating a viable coherent phantom track requires a specified set of the networked radars to detect a consistent position (range and azimuth) and range rate for the phantom

target as it moves along. The methods considered herein to accomplish such a task are restricted to range-delay techniques applied through the radar mainlobe. Obviously, for a team of ECAVs—generally one per radar—attempting to deceive a radar network in such a way, the flyable trajectories of each individual ECAV are restricted to some exclusive range.

Prior work by Pachter and Chandler in Ref. 2 presents a thorough introduction to the cooperative electronic attack problem and mathematically describes the dynamics of a *constant*-speed ECAV given a straight or circular phantom track with *constant* speed. This paper begins by showing through simulation that assuming an ECAV has constant speed severely limits the range of flyable ECAV trajectories given a straight constant-speed phantom track. In response, more general theory for modeling ECAV dynamics mathematically and developing bounds for ECAV trajectories is contributed, which allows for ranges on the ECAV and phantom track speeds as well as limitations on the ECAV antenna operation regions. With these specifications, the flyable ranges for an ECAV given a straight or circular phantom track are developed and verified via simulations. Also, generalized mathematical bounds for a team of ECAVs—*independent* of the phantom track types considered—are provided. One formulation of the decentralized cooperative control problem is supplied as an example, which uses these generalized bounds on ECAV initial conditions and flyable ranges to determine the ECAV team cost versus different phantom tracks in a decentralized fashion.

II. An Explanation of the Deception Problem

Assuming that an ECAV knows the maximum operational range, R_{max}, and location of a radar with pulse-to-pulse agility or discrimination, the ECAV can intercept and appropriately delay the return of the radar's transmitted pulses so that the radar sees a phantom target beyond the ECAV but closer than R_{max}. The capability of digitally storing, altering, and returning encoded pulses so that they correspond to a desired range and range rate is formally known as Digital Radio Frequency Memory (DRFM), but will often be referred to simply as range delay since it is assumed that digital means will be used to accomplish this task; see Ref. 1 for more information. To deceive the radar using only range delay requires that the ECAV be in the radar's mainlobe; of course, the phantom target must also be on the line of sight (LOS) from the radar to the ECAV. Thus, the phantom target's track is a function of the ECAV's range delay and bearing from the radar. If the radar operates at a pulse repetition frequency (PRF) where pulse-delay ranging is performed, then accurately delaying the radar's pulses is crucial. If the radar operates at higher PRFs in track mode, then range information is still important, but the ECAV can focus on sending returns with accurate Doppler frequencies or range rates for the phantom target.

Keep in mind that a phantom track flying roughly perpendicular to a radar will not produce significant Doppler frequencies and may even get filtered out or ignored. Figure 1 illustrates how four ECAVs could cooperatively create a single phantom track to deceive a network of four radars by using range-delay techniques. For this example, where all four of the radars share track files, unless all radars see the same phantom track, the track is dismissed as spurious.

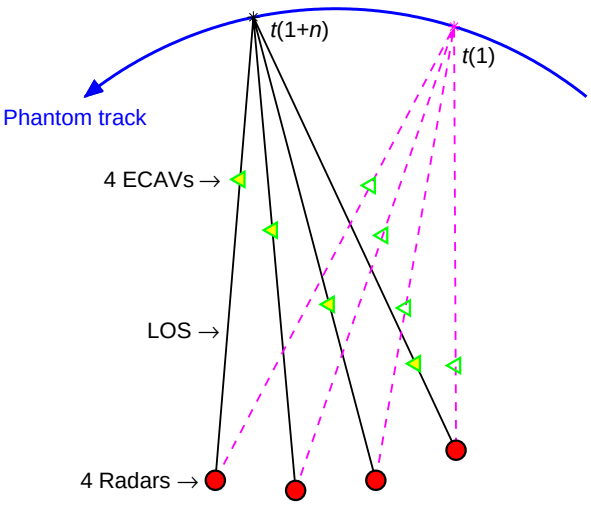

Figure 1. Cooperative mainlobe deception of a radar network by creation of a phantom track.

One problem of interest is to determine the allowable trajectories for the ECAVs given their initial conditions and a time-dependent phantom track. Observing figure 1, one can see that each ECAV behaves much like a bead on a string that is rotating at some variable rate; the ECAV may slide up and down freely but must rotate with the LOS from the radar to the phantom track. If the speed, heading, or another variable of the ECAV is limited, then it may no longer slide freely; in fact, an allowable trajectory for the ECAV might not exist. This idea can also be expressed using the concept of degrees of freedom (DOF). Any general phantom track in the x-y plane has two DOF, which may be represented in polar coordinates by R and θ with reference to a radar as the origin. Likewise, two DOF also represent any free ECAV trajectory in the

same plane and may be represented by r and θ (see figure 2 below). Thus, an ECAV trying to generate a given phantom track will have one constraint, θ, and one DOF. This DOF is then constrained by setting any other ECAV variable.

Mainlobe as opposed to sidelobe deception has the primary advantage in that it is less sophisticated to execute. Its main disadvantage is the ability of producing only one phantom track when the number of ECAVs is equal to the number of networked radars. Other issues that need to be addressed for mainlobe deception include:

- Inaccuracy of radar/ECAV positions and time delay—an estimation problem
- Limitations on ECAV dynamics due to bounded ranges on its speed and antennas and the phantom target speed
- Choosing the "best" phantom track for a team of ECAVs —a decentralized cooperative control problem
- Processing power required by DRFM—can be better at low PRF
- Electronic requirements for generating returns with sufficiently accurate range and Doppler frequency information.

The first issue listed above is the subject of current research but is not addressed below. The second and third issues will be addressed later in more detail.

III. Results of a Constant-Speed ECAV and Phantom Track

UNDERSTANDING first the dynamic limitations imposed on an ECAV when its speed and the phantom track speed are assumed constant will help motivate the later application of realistic bounded ranges for the speed of the ECAV, its region of antenna operation, and the speed of the phantom track. Using mainlobe deception as explained above, assume for now that the ECAV's one DOF is constrained by a constant speed. The inverse problem is now of interest: given a time-dependent phantom track and an ECAV's initial position, synthesize the ECAV trajectory required to create the desired phantom track. For ease of comparison, the following non-dimensional variables are used, with $\upsilon_E = 1$, $R_0 = 1$, and $\theta_0 = 0$.

$$t \to \frac{\upsilon_E}{R_0} t \qquad r \to \frac{r}{R_0}$$
$$\alpha \to \frac{\upsilon_T}{\upsilon_E} \qquad R \to \frac{R}{R_0}$$

Given these definitions and a constant-speed constant-course phantom track for this analysis, figure 2 below illustrates the appropriate variables and their relations. Definitions of the basic ECAV and phantom track variables are also given on the right side of this figure.

The basic equations of motion for the ECAV and phantom target, using polar coordinates, are as follows. Every derivative is taken with respect to time.

$$\dot{r} = \cos\phi_E, \quad r(0) = r_0 \tag{1}$$
$$\dot{\theta} = \frac{1}{r}\sin\phi_E, \quad \theta(0) = 0 \tag{2}$$
$$\dot{R} = \alpha\cos\phi_T, \quad R(0) = 1 \tag{3}$$
$$\dot{\theta} = \alpha\frac{1}{r}\sin\phi_T, \quad \theta(0) = 0 \tag{4}$$

Without loss of generality, $\dot{\theta}$ is assumed positive. Manipulating equations (1) and (2) results in the following differential equations. These same equations easily follow by using the Pythagorean Theorem on figure 2.

$$\dot{r} = \sqrt{1 - (r\dot{\theta})^2}, \quad r(0) = r_0 \tag{5}$$
$$\dot{r} = -\sqrt{1 - (r\dot{\theta})^2}, \quad r(0) = r_0 \tag{6}$$

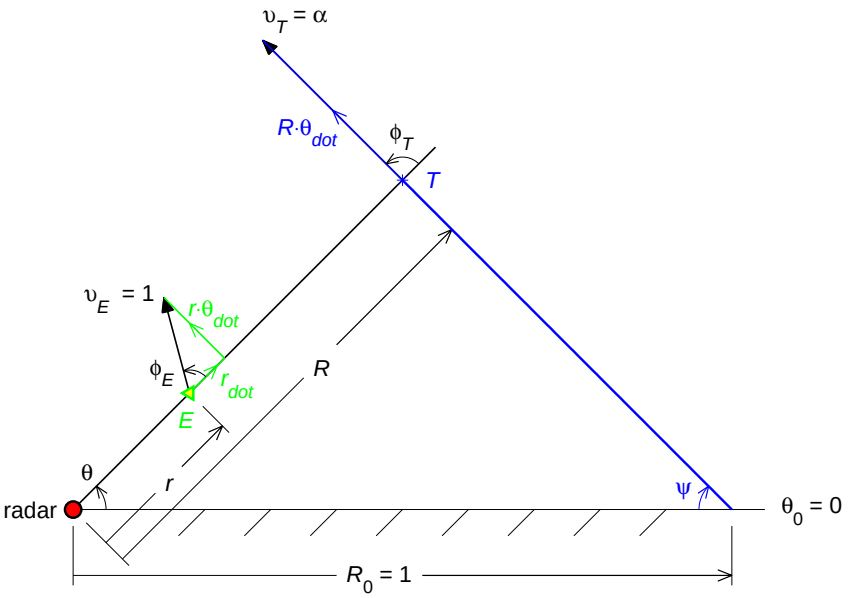

E	ECAV
υ_E	ECAV speed
ϕ_E	ECAV course
r	ECAV range from radar
θ	ECAV/phantom target bearing from radar
T	phantom target
R	phantom target range from radar
υ_T	phantom target speed
ϕ_T	phantom target course
ψ	phantom target heading

Figure 2. Variables and relations for a constant-speed ECAV and a constant-speed constant-course phantom track.

For both equations, the ECAV's range, including r_0, must satisfy the following inequality with $\dot{\theta}$ as a function of time for a solution to exist.

$$r(t) < \frac{1}{\dot{\theta}} \quad \forall t \tag{7}$$

If condition (7) is not satisfied, the solutions to equations (5) and (6) become imaginary. Physically, condition (7) makes it clear that an ECAV cannot fly at a constant speed of one when its range is such that $r\dot{\theta}$ is greater than one (see figure 2 above). If $r\dot{\theta}$ is less than one, the ECAV may fly at a constant speed of one by having the correct $\dot{r}$ component via equation (5) or (6). If either equation (5) or (6) reaches zero in finite time at say t_s, the necessary condition for switching from one equation to the other at t_s is as follows, assuming the second derivative of θ exists.

$$\ddot{\theta}(t_s) = 0 \tag{8}$$

Finally, the equations defining the constant-speed, constant-course phantom track in polar coordinates are as follows (see figure 2 above).

$$R(t) = \sqrt{1 + \alpha^2 t^2 - 2\alpha t \cos\psi} \tag{9}$$

$$\theta(t) = \arcsin\left(\frac{\alpha t \sin\psi}{R(t)}\right) \tag{10}$$

$$\dot{\theta}(t) = \frac{\alpha \sin\psi}{1 + \alpha^2 t^2 - 2\alpha t \cos\psi} \tag{11}$$

To solve for an ECAV trajectory given this phantom track, equation (11) is inserted into equation (5) or (6), and the solution, $r(t)$, is plotted versus $\theta(t)$, which is obtained from equations (10) and (9). A good portion of the mathematical development given above is from Ref. 2.

Figures 3 and 4 below effectively explore equations (5) and (6) by plotting ECAV trajectory solutions for various initial conditions. For each equation/figure, the initial conditions are selected to show the minimum and maximum r_0 values yielding a flyable ECAV trajectory for a full 90 degrees, and also one initial condition or r_0 value where the trajectory runs into the bound represented by condition (7) before $\theta = 90$ degrees is reached. In both figures, the maximum valid value for r_0 yields an ECAV trajectory that switches from equation (5) to (6) or vice versa at $\theta = 45$ degrees.

From observing Figures 3 and 4, the sets of initial conditions yielding complete ECAV trajectories for a full 90 degrees (valid initial conditions) are small compared to the set $[0, 0.707]$, which contains all the initial

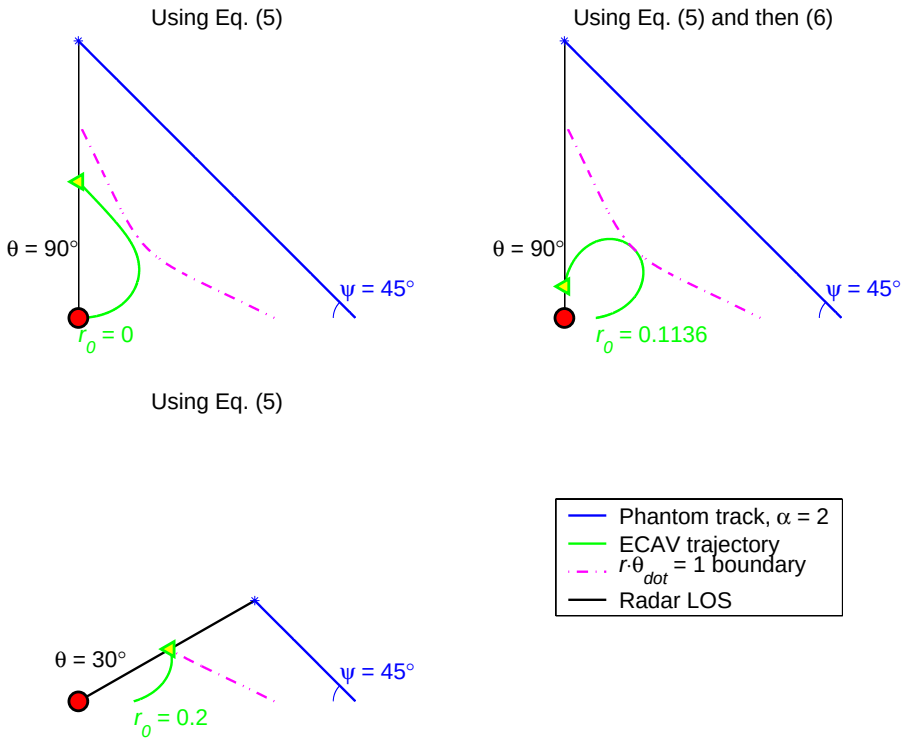

Figure 3. Constant-speed ECAV trajectory solutions for a constant-speed, constant-course phantom track, starting with equation (5).

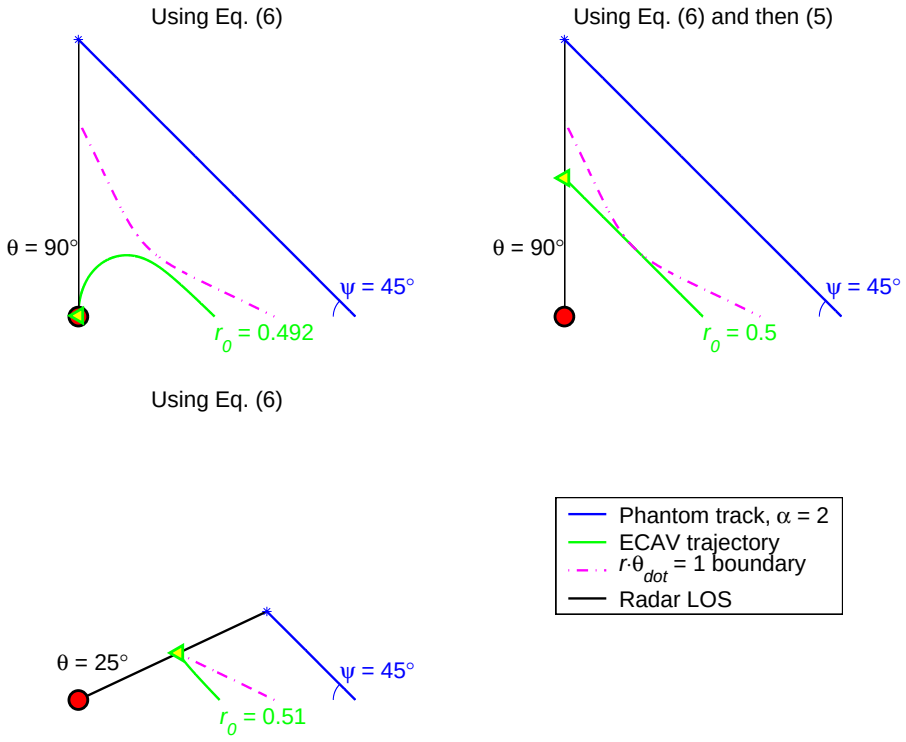

Figure 4. Constant-speed ECAV trajectory solutions for a constant-speed, constant-course phantom track, starting with equation (6).

conditions an ECAV could *start deceiving* the radar from for $\alpha = 2$. In addition, these results are for no additional limitations on the ECAV dynamics. The set size of these valid initial conditions varies predictably with both phantom track speed and heading, but this observation is not pursued. The main point here is that the constant-speed limitations on the ECAV and phantom track must be relaxed to a realistic range to allow the ECAV more flexibility in choosing its starting point and trajectory in the deception process.

IV. General Theory for ECAV Trajectory Bounds and Solutions

Because the assumption of a constant-speed ECAV and phantom track puts severe limitations on the ECAV valid initial conditions and trajectories, it is beneficial to move the scenario closer to reality by allowing the ECAV and phantom track speeds to vary within some bounded range. In addition, it is now assumed that the ECAV has two fixed antennas—each mounted on one side of the ECAV with less than a 90-degree look-angle from its central axis. Hence, the ECAV can no longer send pulse returns to a radar at any course angle, ϕ_E.

Mainlobe deception is again assumed, so the ECAV has one DOF, which will be constrained in different ways to create several ECAV dynamic systems for exploration of the ECAV's flyable range given a phantom track. For ease of comparison, the following non-dimensional variables are used, with $v_{Em} = 1$ (average/nominal ECAV speed), $R_0 = 1$, and $\theta_0 = 0$.

$$t \to \frac{v_{Em}}{R_0} t \qquad r \to \frac{r}{R_0}$$
$$\alpha \to \frac{v_T}{v_{Em}} \qquad R \to \frac{R}{R_0}$$
$$v_E \to \frac{v_E}{v_{Em}}$$

For the rest of this study, the following physically realistic ranges are used in determining ECAV trajectory bounds and solutions.

$$\begin{aligned} v_E &\sim \pm 20\% \\ \phi_E &\sim 90^\circ \pm 60^\circ \\ \alpha &\sim \pm 20\% \end{aligned}$$

Given the definitions and the ranges for v_E, ϕ_E, and α listed above, the minimum and maximum values for these same variables are as follows.

$$\begin{aligned} v_{Emin} &= 0.8 & \phi_{Emin} &= \frac{\pi}{6} & \alpha_{min} &= 0.8\alpha \\ v_{Emax} &= 1.2 & \phi_{Emax} &= \frac{5\pi}{6} & \alpha_{max} &= 1.2\alpha \end{aligned} \tag{12}$$

Now for a *generic* phantom track and the previously defined non-dimensional variables, the appropriate variables and their relations for the track and for developing ECAV dynamic systems are shown below in figure 5. Definitions of the basic ECAV and phantom track variables are also given on the right side of this figure.

The basic equations of motion for the ECAV and phantom target, using polar coordinates, are as follows. Every derivative is taken with respect to time. An equation for ECAV time delay, t_d, is also included.

$$\dot{r} = v_E \cos\phi_E, \quad r(0) = r_0 \tag{13}$$
$$\dot{\theta} = \frac{v_E}{r} \sin\phi_E, \quad \theta(0) = 0 \tag{14}$$
$$\dot{R} = \alpha \cos\phi_T, \quad R(0) = 1 \tag{15}$$
$$\dot{\theta} = \frac{\alpha}{r} \sin\phi_T, \quad \theta(0) = 0 \tag{16}$$
$$t_d(t) = \frac{c}{2}\left(R(t) - r(t)\right) \tag{17}$$

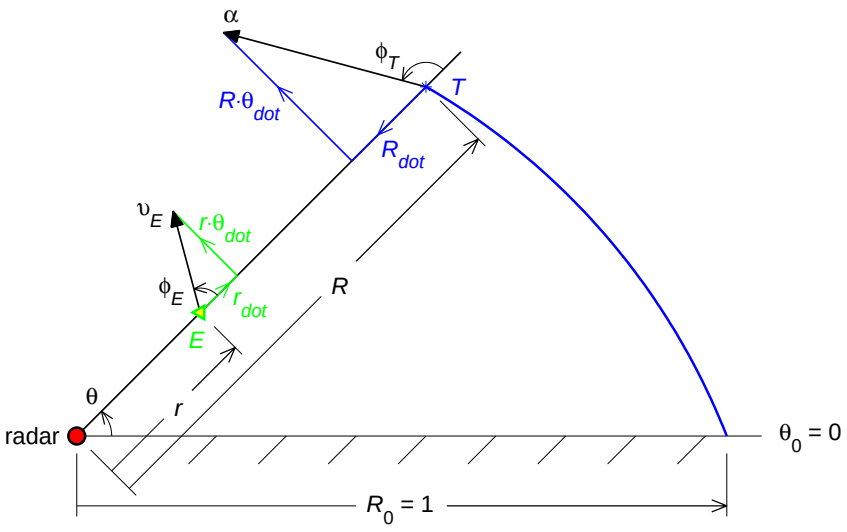

E	ECAV
υ_E	ECAV speed
ϕ_E	ECAV course
r	ECAV range from radar
θ	ECAV/phantom target bearing from radar
T	phantom target
R	phantom target range from radar
υ_T	phantom target speed
ϕ_T	phantom target course

Figure 5. Variables and relations for an ECAV with variable speed and a generic phantom track with variable speed.

Without loss of generality, $\dot{\theta}$ is assumed positive and given by some pre-determined phantom track. Six ECAV dynamic systems are now presented below, which can each be developed from equations (13) and (14) by setting one ECAV variable. All systems include an algorithm for choosing initial conditions that satisfy the ranges in (12), ODEs (ordinary differential equations) necessary to solve for the ECAV trajectory, and bounds resulting from (12) that must be satisfied for all time. A subscript c indicates that the corresponding variable is constant. Remember that $\dot{\theta}$ is a function of time.

A. Constant Speed System (υ_{Ec})

For the initial conditions, choose υ_{Ec} and r_0 in sequence to satisfy the following initial constraints.

$$\upsilon_{Emin} \le \upsilon_{Ec} \le \upsilon_{Emax}$$

$$\frac{\upsilon_{Ec} \sin\phi_{Emin}}{\dot{\theta}_0} \le r_0 \le \frac{\upsilon_{Ec}}{\dot{\theta}_0}$$

Then the differential equation with $(+)$ and/or $(-)$ to be solved is given as

$$\dot{r} = \begin{cases} +\sqrt{{\upsilon_{Ec}}^2 - (r\dot{\theta})^2} \\ -\sqrt{{\upsilon_{Ec}}^2 - (r\dot{\theta})^2} \end{cases}, \quad r(0) = r_0, \tag{18}$$

where for the solution $r(t)$, the course constraint

$$\sin\phi_{Emin} \le \frac{r(t)\dot{\theta}}{\upsilon_{Ec}} \quad \forall t$$

must be satisfied, and the constraint

$$s(t) := {\upsilon_{Ec}}^2 - (r(t)\dot{\theta})^2 > 0 \quad \forall t$$

must also be satisfied; however, if $s(t) = 0$ and condition (8) is satisfied, then switching to solving the other half of equation (18) is valid.

B. Constant Course System (ϕ_{Ec})

For the initial conditions, choose ϕ_{Ec} and r_0 in sequence to satisfy the following initial constraints.

$$\phi_{Emin} \leq \phi_{Ec} \leq \phi_{Emax}$$
$$\frac{\upsilon_{Emin} \sin \phi_{Ec}}{\dot{\theta}_0} \leq r_0 \leq \frac{\upsilon_{Emax} \sin \phi_{Ec}}{\dot{\theta}_0}$$

Then the differential equation to be solved is given as

$$\dot{r} = r\dot{\theta} \cot \phi_{Ec}, \quad r(0) = r_0, \tag{19}$$

where for the solution $r(t)$, the speed constraint

$$\upsilon_{Emin} \leq \frac{r(t)\dot{\theta}}{\sin \phi_{Ec}} \leq \upsilon_{Emax} \quad \forall t$$

must be satisfied.

C. Constant Heading System (h_{Ec})

For the initial conditions, choose h_{Ec} and r_0 in sequence to satisfy the following initial constraints.

$$\phi_{Emin} + \theta_0 \leq h_{Ec} \leq \phi_{Emax} + \theta_0$$
$$\frac{\upsilon_{Emin} \sin (h_{Ec} - \theta_0)}{\dot{\theta}_0} \leq r_0 \leq \frac{\upsilon_{Emax} \sin (h_{Ec} - \theta_0)}{\dot{\theta}_0}$$

Then the differential equation to be solved is given as

$$\dot{r} = r\dot{\theta} \cot(h_{Ec} - \theta(t)), \quad r(0) = r_0, \tag{20}$$

where for the solution $r(t)$, the speed constraint

$$\upsilon_{Emin} \leq \frac{r(t)\dot{\theta}}{\sin \phi_E(t)} \leq \upsilon_{Emax} \quad \forall t$$

must be satisfied.

D. Constant Speed Rate System ($\dot{\upsilon}_{Ec}$)

For the initial conditions, choose $\dot{\upsilon}_{Ec}$, υ_{E0}, and r_0 in sequence to satisfy the following initial constraints.

$$\dot{\upsilon}_{Emin} \leq \dot{\upsilon}_{Ec} \leq \dot{\upsilon}_{Emax}$$
$$\upsilon_{Emin} \leq \upsilon_{E0} \leq \upsilon_{Emax}$$
$$\frac{\upsilon_{E0} \sin \phi_{Emin}}{\dot{\theta}_0} \leq r_0 \leq \frac{\upsilon_{E0}}{\dot{\theta}_0}$$

Then the differential equation to be solved is given as

$$\ddot{r} = \frac{-r\dot{\theta}(r\ddot{\theta} + \dot{r}\dot{\theta}) + \upsilon_E(t)\dot{\upsilon}_{Ec}}{\dot{r}}, \qquad \begin{matrix} r(0) = r_0 \\ \dot{r}(0) = \dot{r}_0 = \sqrt{{\upsilon_{E0}}^2 - (r_0\dot{\theta}_0)^2} \end{matrix}, \tag{21}$$

where for the solution $r(t)$, the speed constraint

$$\upsilon_{Emin} \leq \upsilon_E(t) \leq \upsilon_{Emax} \quad \forall t$$

must be satisfied, the course constraint

$$\sin \phi_{Emin} \leq \frac{r(t)\dot{\theta}}{\upsilon_E(t)} \quad \forall t$$

must be satisfied, and the constraint

$$s(t) := |\dot{r}(t)| > 0 \quad \forall t$$

must also be satisfied; however, if $s(t) = 0$, then switching to $-\dot{\upsilon}_{Ec}$ and perturbing $\dot{r}$ across zero allows the solution of equation (21) to continue.

E. Constant Turn Rate System ($\dot{h}_{Ec}$)

For the initial conditions, choose $\dot{h}_{Ec}$ and then ϕ_{E0} and r_0 in sequence to satisfy the following initial constraints.

$$\phi_{Emin} \leq \phi_{E0} \leq \phi_{Emax}$$
$$\frac{\upsilon_{Emin} \sin\phi_{E0}}{\dot{\theta}_0} \leq r_0 \leq \frac{\upsilon_{Emax} \sin\phi_{E0}}{\dot{\theta}_0}$$

Then the differential equation to be solved is given as

$$\ddot{r} = \frac{\dot{r}(r\ddot{\theta} + \dot{r}\dot{\theta}) - {\upsilon_E}^2(t)(\dot{h}_{Ec} - \dot{\theta})}{r\dot{\theta}}, \qquad \begin{matrix} r(0) = r_0 \\ \dot{r}(0) = \dot{r}_0 = r_0\dot{\theta}_0 \cot\phi_{E0} \end{matrix} , \tag{22}$$

where for the solution $r(t)$, the speed constraint

$$\upsilon_{Emin} \leq \upsilon_E(t) \leq \upsilon_{Emax} \quad \forall t$$

must be satisfied, and the course constraint

$$\sin\phi_{Emin} \leq \frac{r(t)\dot{\theta}}{\upsilon_E(t)} \quad \forall t$$

must be satisfied.

F. Constant Acceleration System (a_{Ec})

For the initial conditions, choose a_{Ec} and then υ_{E0} and r_0 in sequence to satisfy the following initial constraints.

$$\upsilon_{Emin} \leq \upsilon_{E0} \leq \upsilon_{Emax}$$
$$\frac{\upsilon_{E0} \sin\phi_{Emin}}{\dot{\theta}_0} \leq r_0 \leq \frac{\upsilon_{E0}}{\dot{\theta}_0}$$

Then the differential equation with $(+)$ and/or $(-)$ parts to be solved is given as

$$\dot{r} = \begin{cases} r\dot{\theta}^2 + \sqrt{{a_{Ec}}^2 - (r\ddot{\theta} + 2\dot{r}\dot{\theta})^2} \\ r\dot{\theta}^2 - \sqrt{{a_{Ec}}^2 - (r\ddot{\theta} + 2\dot{r}\dot{\theta})^2} \end{cases} , \qquad \begin{matrix} r(0) = r_0 \\ \dot{r}(0) = \dot{r}_0 = \sqrt{{\upsilon_{E0}}^2 - (r_0\dot{\theta}_0)^2} \end{matrix} , \tag{23}$$

where for the solution $r(t)$, the speed constraint

$$\upsilon_{Emin} \leq \upsilon_E(t) \leq \upsilon_{Emax} \quad \forall t$$

must be satisfied, the course constraint

$$\sin\phi_{Emin} \leq \frac{r(t)\dot{\theta}}{\upsilon_E(t)} \quad \forall t$$

must be satisfied, and the constraint

$$s(t) := {a_{Ec}}^2 - (r(t)\ddot{\theta} + 2\dot{r}\dot{\theta})^2 > 0 \quad \forall t$$

must also be satisfied.

System A above simply contains a reformulation of equations (5) and (6) for a range of constant ECAV speeds. System B allows the choice of a constant ECAV course, which is actually relative to θ (see figure 5 above); a course of 90 degrees would result in a circular trajectory. Equation (19) in system B may actually be solved explicitly for $r(t)$, but this solution is not a concern. System C allows the choice of a constant ECAV heading, which means that the ECAV will fly in a straight line with the specified heading. Equation (20) may also be solved explicitly for $r(t)$ if the system is autonomous, i.e. if θ is not a function of time. System D allows the choice of a constant ECAV speed rate and is not too useful since $s(t)$ quickly reaches zero for most initial conditions. System E allows the choice of a constant ECAV turn rate and is extremely useful

because it can often be used to find the minimum and maximum initial conditions for which a flyable ECAV trajectory exists for a specified range of θ. System F allows the choice of a constant ECAV acceleration (time derivative of ECAV velocity) and is more useful when a given phantom track is circular in form so that a constant acceleration greater (less) than the inherent centripetal acceleration causes the ECAV to spiral in (out) relative to the radar.

The variable definitions and minimum/maximum values for ECAV speed and course in (12) give rise to the following $r\dot{\theta}$-boundary lines for the ECAV, which are similar in concept to condition (7) with a constant-speed ECAV.

$$r(t) = \frac{v_{Emin}}{\dot{\theta}} = \frac{0.8}{\dot{\theta}} \tag{24}$$

$$r(t) = \frac{v_{Emax}}{\dot{\theta}} = \frac{1.2}{\dot{\theta}} \tag{25}$$

$$r(t) = \frac{v_{Emin}\sin\phi_{Emin}}{\dot{\theta}} = \frac{0.4}{\dot{\theta}} \tag{26}$$

$$r(t) = \frac{v_{Emax}\sin\phi_{Emin}}{\dot{\theta}} = \frac{0.6}{\dot{\theta}} \tag{27}$$

The ECAV's range may not exceed boundary (25) at any time because this would require it to fly faster than its maximum speed. If the ECAV range decreases below boundary (24), the ECAV may continue its trajectory, but may not fly perpendicular to its current LOS since it must have a nonzero $\dot{r}$-component to fly above its minimum speed. The ECAV's range may not decrease below boundary (26) at any time because this would rotate its fixed antennas out of range of the radar even at minimum speed. If the ECAV range decreases below boundary (27), the ECAV may continue its trajectory, but only at a speed less than its maximum speed.

For this analysis on ECAV trajectory bounds, it is beneficial to convert the phantom target speed range into a larger pseudo-range for the ECAV speed with the phantom target speed resumed to a virtual constant. To make this conversion, the effect on the $r\dot{\theta}$-boundary lines (24)–(27) due to varying α down to α_{min} and up to α_{max} is determined and maximized to produce a new set of $r\dot{\theta}$-boundary lines for the ECAV speed pseudo-range. Hence, the effect of α on $\dot{\theta}$ must first be determined for various phantom tracks. The dependence of $\dot{\theta}$ on α for a straight phantom track is given as follows, using equations (9)–(11), with $\dot{\theta}$ solved explicitly as a function of θ.

$$\dot{\theta}(\theta) = \frac{\alpha\sin\psi}{1 + \left(\frac{\sin\theta}{\sin(\pi-\psi-\theta)}\right)^2 - 2\cos\psi\frac{\sin\theta}{\sin(\pi-\psi-\theta)}} \tag{28}$$

Conveniently, $\dot{\theta}$ is directly proportional to α for any given value of θ, and this result can graphically be shown to hold true also when the phantom track is circular and referenced to a radar not at its center as in equations (42)–(44) below. Therefore, the new $r\dot{\theta}$-boundary lines are as follows for a straight or circular phantom track, where v_{Epsmin} and v_{Epsmax} are *defined* in equations (29) and (30), respectively.

$$r(t) = \frac{v_{Emin}}{(\alpha_{max}-\alpha)\dot{\theta}} =: \frac{v_{Epsmin}}{\dot{\theta}} = \frac{0.67}{\dot{\theta}} \tag{29}$$

$$r(t) = \frac{v_{Emax}}{(\alpha-\alpha_{min})\dot{\theta}} =: \frac{v_{Epsmax}}{\dot{\theta}} = \frac{1.5}{\dot{\theta}} \tag{30}$$

$$r(t) = \frac{v_{Epsmin}\sin\phi_{Emin}}{\dot{\theta}} = \frac{0.33}{\dot{\theta}} \tag{31}$$

$$r(t) = \frac{v_{Epsmax}\sin\phi_{Emin}}{\dot{\theta}} = \frac{0.75}{\dot{\theta}} \tag{32}$$

Figure 6 below is an exported frame from a MATLAB-generated video and illustrates visually how $r\dot{\theta}$-boundaries (24) and (25) are changed to $r\dot{\theta}$-boundaries (29) and (30), respectively, by allowing variation in α to move the ECAV speed range in or out to further limits. This visual explanation is similar for the changes made to convert boundaries (26) and (27) to boundaries (31) and (32), respectively.

In figure 6, the gray boundary represents the outer limit where α is decreased by 20% to α_{min}, which effectively moves the black boundary range for $\upsilon_E \pm 20\%$ (the area between the black curves) out to the gray boundary; at this point, the outer black boundary coincides with the gray boundary. Likewise, the cyan boundary represents the inner limit where the black boundary range may be moved when α is increased by 20% to α_{max}. It is important to realize that these ultimate lower and upper $r\dot{\theta}$-boundaries (the cyan and gray curves) may not coexist at any instant in time because α may only be one value at any time. This fact is important primarily in the case of multiple ECAVs and multiple radars because it constrains all ECAVs to be within the υ_E-boundary range (the area between the black curves) at any given time, even though that range may move in *or* out as shown in figure 6. When changing α to accommodate an ECAV's desired position or speed, α will have to modulate in a continuous and believable fashion, especially if the radar is operating at a high PRF.

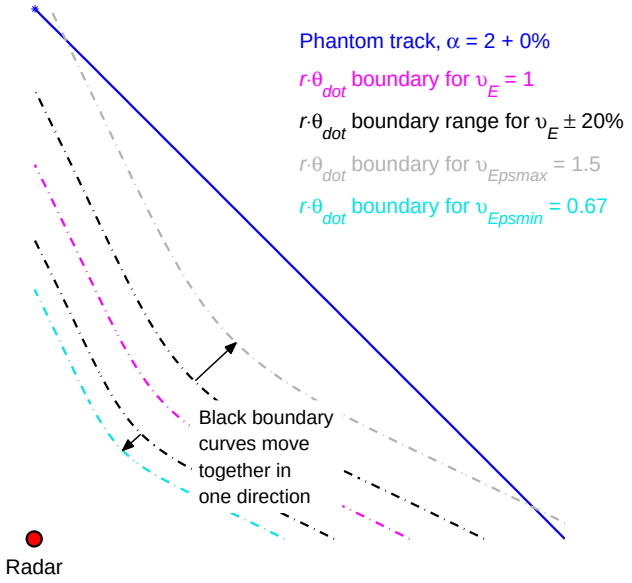

Figure 6. Conversion of phantom track speed range into larger ECAV speed pseudo-range.

To further enhance the assessment of an ECAV's flyable range given a phantom track and some range of θ, the following speed isolines may also be used, where $R(t)$ is specified by the phantom track being created.

$$r(t) = \frac{\upsilon_{Epsmin}}{\alpha} R(t) \tag{33}$$

$$r(t) = \frac{\upsilon_{Epsmax}}{\alpha} R(t) \tag{34}$$

V. ECAV Bounds for a Straight Phantom Track

THE theory presented in the previous section for treating ranges on ECAV speed, course (region of antenna operation), and the speed of the phantom track is now utilized to conduct a survey of the ECAV bounds for a constant-course phantom track through the solution of ordinary differential equations. The parametric equations for this straight phantom track, taken from Ref. 2, are shown below in polar coordinates and are identical to equations (9)–(11).

$$R(t) = \sqrt{1 + \alpha^2 t^2 - 2\alpha t \cos\psi} \tag{35}$$

$$\theta(t) = \arcsin\left(\frac{\alpha t \sin\psi}{R(t)}\right) \tag{36}$$

$$\dot{\theta}(t) = \frac{\alpha \sin\psi}{1 + \alpha^2 t^2 - 2\alpha t \cos\psi} \tag{37}$$

Using equations (35)–(37) and with $\alpha = 2$ and $\psi = 45$ degrees, a phantom track is plotted along with the boundaries and isolines corresponding to (29)–(32) and (33)–(34), respectively, in figure 7 below. The yellow lines represent a flyable ECAV range for $\theta = 90$ degrees. This flyable range represents the union of all positions the ECAV could visit on certain trajectories and still be able to create a phantom track through 90 degrees.

Many ECAV trajectories—solved using the six dynamic systems A through F presented in the previous section—were used to test and verify the results shown in figure 7. The flyable range bounded by the pseudo-speed isolines is valid since any trajectory parallel to and between these two isolines is within the ECAV speed pseudo-range and course range. The additional part of the flyable range, defined where the green curves are less than the $\upsilon_E = 0.67$ isoline, is actually bounded by a (minimum) constant-speed ECAV

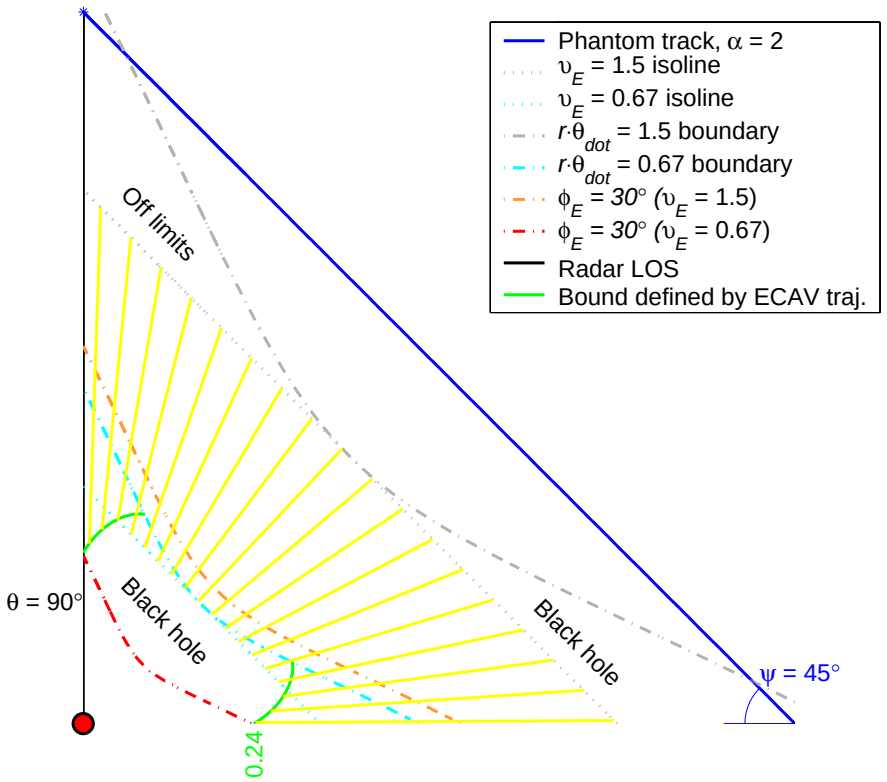

Figure 7. ECAV flyable range for a constant-course phantom track, $\theta = 90$ degrees.

trajectory solution using system A, where the ECAV is initially/finally on the red boundary, i.e. its course is at ϕ_{Emin} for both $\theta = 0$ and $\theta = 90$ degrees. For an ECAV starting on the right trajectory curve and running into the $r\dot{\theta} = 0.67$ boundary, it could then switch to a different system—such as system B with $\phi_{Ec} = 90$ degrees—to create a circular trajectory and then switch back to the constant speed system with $\upsilon_{Ec} = 0.67$ when it again reached the boundary. This line of reasoning as well as many flyable ECAV trajectories produced using a constant turn rate with system E provide ample evidence for the flyable range below the speed isolines in figure 7.

The right "black hole" in figure 7 is an area that can be entered by the ECAV, but once the ECAV is in this region, it cannot exit back into the flyable range; it will run into the $r\dot{\theta} = 1.5$ boundary and stop. To explain this mathematically, the following equation for the ECAV speed at any time instance is used.

$$\upsilon_E = \sqrt{\dot{r}^2 + (r\dot{\theta})^2} \tag{38}$$

Taking a point on the $\upsilon_E = 1.5$ isoline that bounds the black hole, if the absolute value of $\dot{r}$ is decreased, which corresponds to entering the black hole, then equation (38) says that υ_E will also decrease. This allows the ECAV to enter the black hole because in doing so it will be flying within its speed pseudo-range or below υ_{Epsmax}. However, for an ECAV to exit, the absolute value of $\dot{r}$ would have to increase, which by equation (38) requires that the ECAV fly faster than its maximum pseudo-speed of 1.5. A similar argument can be used to show that the region labeled "off limits" is an area that can be exited by the ECAV but not entered from its flyable range. The left "black hole" is an area that, once entered, will require that the ECAV turn in towards the radar at a progressive rate to stay within its speed pseudo-range; at some point in this process, the ECAV will reach its course bound between the orange and red curves where its fixed antennas rotate out of range of the radar—all before $\theta = 90$ degrees is reached.

In addition to the speed and course bounds discussed above, there exist ultimate θ-bounds on ECAV trajectories given a straight phantom track. For an ECAV flying parallel to a speed isoline, it would reach its course bound or antenna limit at 60 degrees off of the shortest LOS from the radar to the phantom track. This corresponds directly to the range chosen for ϕ_E in the previous section, which is 90 ± 60 degrees. It

may be possible for the ECAV to continue the phantom track for slightly greater values of θ by starting on a high speed isoline and turning in towards the radar right before it reaches its course bound; however, this possibility was not explored.

The analysis in this section is modular in that it is applicable to any number of ECAVs and the same number of radars, each on an individual basis. The parameter ψ of the phantom track is simply calculated for each radar, and a different set of modified phantom track equations are then used for each radar/ECAV pair so that together the team creates one coherent straight phantom track with speed α.

VI. ECAV Bounds for a Simple Circular Phantom Track

The general theory for ECAV trajectory bounds and solutions is again utilized to conduct a survey of the ECAV bounds for a circular phantom track with the radar placed at the circle's center. The equations for this type of phantom track, taken from Ref. 2, are shown below in polar coordinates.

$$R(t) \equiv 1 \tag{39}$$

$$\theta(t) = \alpha t \tag{40}$$

$$\dot{\theta}(t) \equiv \alpha \tag{41}$$

With equations (39)–(41) representing the circular phantom track, ECAV systems A through F are now autonomous and may be analyzed in the phase plane if so desired. Because of this simplification, the simple circular phantom track presents a good opportunity to more thoroughly analyze the ECAV dynamic systems A through F. Using equations (39)–(41) and with $\alpha = 2$, a phantom track is plotted along with the boundaries corresponding to (29)–(32) in figure 8 below. The yellow lines represent a flyable ECAV range for $\theta = 180$ degrees. This flyable range represents the union of all positions the ECAV could visit on certain trajectories and still be able to create a phantom track through 180 degrees.

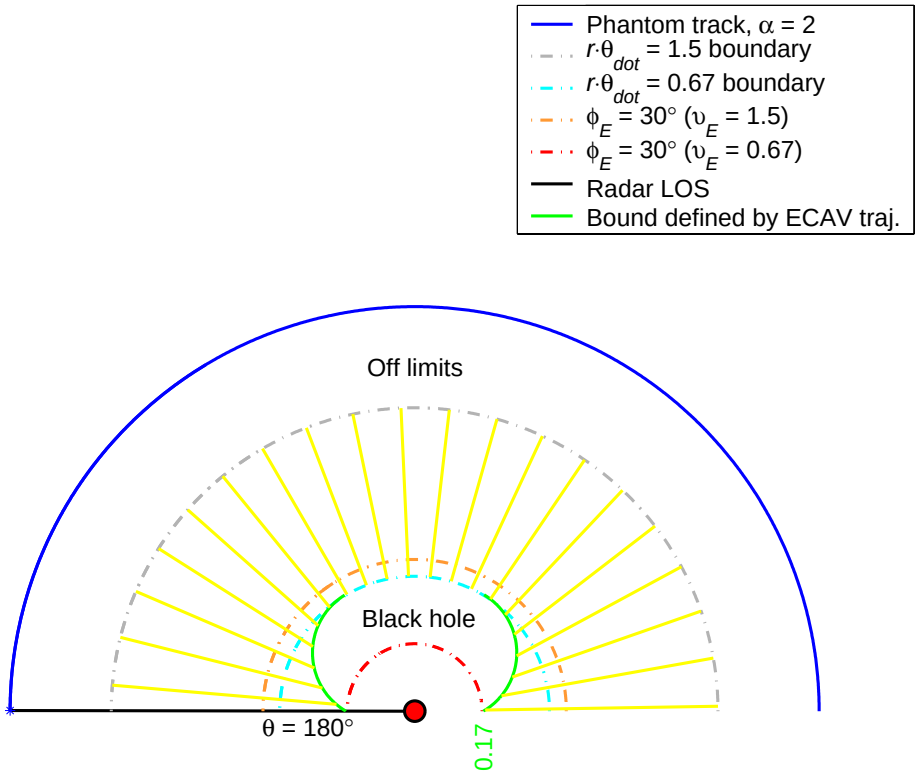

Figure 8. ECAV flyable range for a simple circular phantom track and $\theta = 180$ degrees.

Many ECAV trajectories—solved using the six dynamic systems A through F presented earlier—were used to test and verify the results shown in figure 8. For the simple circular phantom track, the minimum

and maximum pseudo-speed isolines are not identified because they coincide with the $r\dot{\theta} = 0.67$ and $r\dot{\theta} = 1.5$ boundaries, respectively; this is advantageous because it means that the ECAV has no ultimate θ-bounds as with the straight phantom track. Justification for the flyable range presented above in figure 8 is not presented here because the simple circular phantom track is actually a special case of the general circular phantom track, which is presented in the next section.

The region labeled "off limits" in figure 8 is an area that cannot be entered or exited by the ECAV because it is bounded by $r\dot{\theta} = 1.5$. Taking a point on this boundary, to enter or exit the off limits region requires $\dot{r}$ to be nonzero, which increases the ECAV speed above its pseudo-maximum according to equation (38). The "black hole" is an area that, once entered, will require that the ECAV turn in towards the radar at a progressive rate to stay within its speed pseudo-range; at some point in this process, the ECAV will reach its course bound between the orange and red curves where its fixed antennas rotate out of range of the radar—all before $\theta = 180$ degrees is reached.

Although simple and useful for understanding ECAV systems and trajectory bounds, the analysis in this section alone is not modular. It is applicable to only one ECAV trying to deceive a radar located at the center of the circular phantom track. However, this information combined with the general circular phantom track analysis presented in the next section will provide the modularity needed for a team of ECAVs to create one coherent circular phantom track for a radar network.

VII. ECAV Bounds for a General Circular Phantom Track

The general theory for ECAV trajectory bounds and solutions is once more utilized to conduct a survey of the ECAV bounds for a circular phantom track with the radar placed arbitrarily with reference to the circle's center. The equations for this type of phantom track are shown below in polar coordinates. Only two of the phantom track's three additional parameters, a, b, and ρ, must be specified; a and b represent the horizontal and vertical distances from the circle center to the radar.

$$R(t) = \sqrt{1 + 2a\rho - 2a\rho\cos\frac{\alpha}{\rho}t - 2b\rho\sin\frac{\alpha}{\rho}t} \tag{42}$$

$$\theta(t) = \operatorname{sgn}\left(\xi - \frac{\alpha}{\rho}t\right)(\chi(t) - \pi) + \xi, \quad \pi - \xi \le t \le \pi + \xi \tag{43}$$

$$\dot{\theta}(t) = \frac{\alpha}{R^2(t)}\left(\rho - a\cos\frac{\alpha}{\rho}t - b\sin\frac{\alpha}{\rho}t\right) \tag{44}$$

The mathematical definitions for $\chi(t)$ and the parameters ρ and ξ are as follows.

$$\chi(t) = \arg\left(\rho\left|a\sin\frac{\alpha}{\rho}t - b\cos\frac{\alpha}{\rho}t\right|, a^2 + b^2 - a\rho\cos\frac{\alpha}{\rho}t - b\rho\sin\frac{\alpha}{\rho}t\right)$$

$$\rho = a + \sqrt{1 - b^2}$$

$$\xi = \arg(b, a)$$

Using equations (42)–(44) and with $\alpha = 2$, $a = -0.38$, and $b = 0.22$ (radar placed inside the circle), a phantom track is plotted along with the boundaries and isolines corresponding to (29)–(32) and (33)–(34), respectively, in figure 9 below. The yellow lines represent a flyable ECAV range for a circular phantom track of 180 degrees, which corresponds to $\theta = 227$ degrees. This flyable range represents the union of all positions the ECAV could visit on certain trajectories and still be able to create a 180-degree circular phantom track.

Many ECAV trajectories—solved using dynamic systems A and E presented earlier—were used to test and verify the results shown in figure 9. For the general circular phantom track, the relevant isolines and boundaries plotted in figure 9 look similar to those plotted for the straight phantom track (see figure 7 above) except curved around in an egg-like shape. The flyable range bounded by the speed isolines is valid since any ECAV trajectory coinciding with a v_E-isoline between these two will fly at a constant speed and be within the ECAV speed pseudo-range and course range. The additional part of the flyable range, defined where the green curves are less than the $v_E = 0.67$ isoline, is actually bounded by a (minimum) constant-speed ECAV trajectory solution using system A, where the ECAV is initially/finally on the red boundary, i.e. its course is at ϕ_{Emin} for both $\theta = 0$ and $\theta = 90$ degrees. For an ECAV starting on the right trajectory curve and running into the $r\dot{\theta} = 0.67$ boundary, it could then turn into an appropriate speed isoline in between

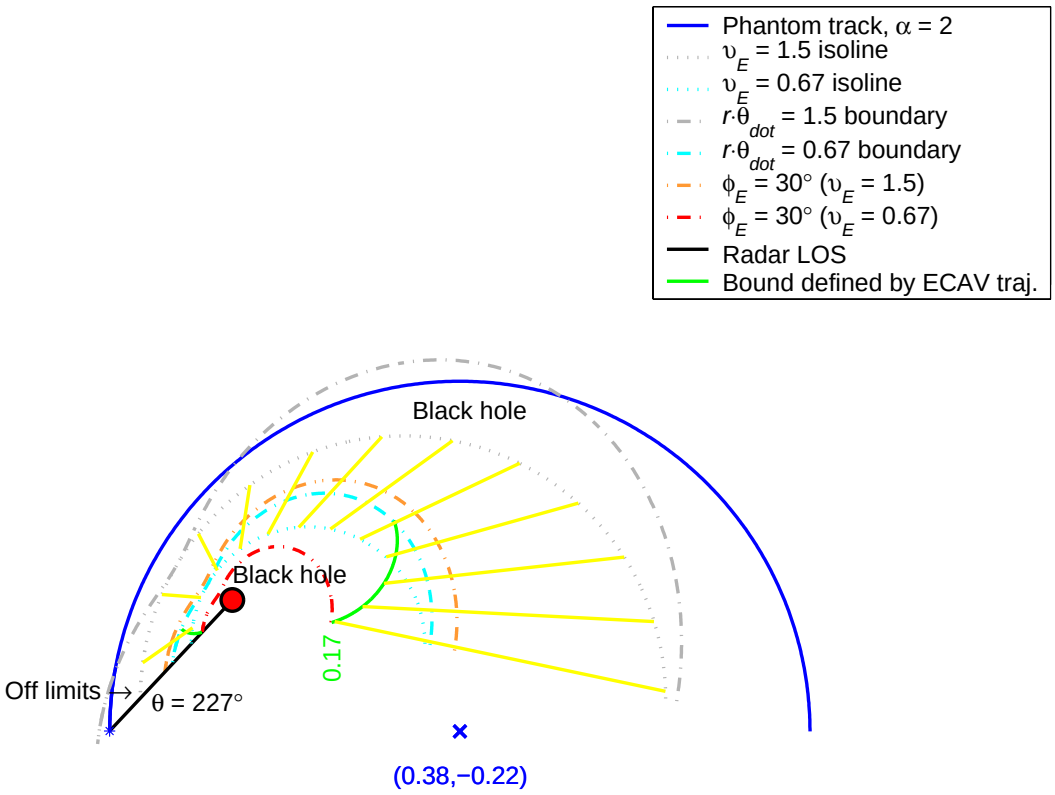

Figure 9. ECAV flyable range for a general 180-degree circular phantom track with the radar placed inside the circle.

the minimum and maximum isolines and switch back to the constant velocity system with $\upsilon_{Ec} = 0.67$ when it again reached the boundary. This line of reasoning as well as some flyable ECAV trajectories produced using a constant turn rate with system E provide evidence for the flyable range below the speed isolines in figure 9. It has been verified that mirroring the radar's location about the phantom circle center's y-axis (vertical axis) produces symmetric bounds and flyable ECAV trajectories about this axis.

The "black hole" and "off limits" regions are analogous to those shown for the straight phantom track in figure 7 above. Their explanations are likewise similar and so are omitted.

Note that choosing the radar outside the circular path of the phantom track will severely limit how long in time or θ the phantom track may be generated. When the phantom track heading comes close to pointing towards the radar ($\dot{\theta}$ close to zero), creation of the track will stop. This result is due to the course/antenna bounds imposed on the ECAV.

The analysis in this section, combined with that for the simple circular phantom track in the previous section, now provides a modular approach for a circular phantom track applicable to any number of ECAVs and the same number of radars, each on an individual basis. The parameters a and b of the phantom track are simply recalculated for each radar, and a different set of modified phantom track equations are then used for each radar/ECAV pair so that together the team creates one coherent circular phantom track with speed α. However, if any radar is placed outside the circular phantom track, the track will be generated for less than 180 degrees due to the ECAVs' course/antenna limitations from (12).

VIII. General Bounds for ECAV Initial Conditions and Flyable Ranges

Based on the ECAV flyable ranges developed for straight and circular phantom tracks and presented in figures 7 through 9 above, the following equations define and summarize the range of valid initial conditions for an individual i^{th} ECAV to start from and generate a straight or circular phantom track for a desired range of θ, where R_{0i} is a dimensional length.

$$(r_{0min})_i = \frac{\upsilon_{Epsmin} \sin\phi_{Emin}}{\dot{\theta}_{0i}} R_{0i} \tag{45}$$

$$(r_{0max})_i = \min\left(\frac{\upsilon_{Epsmax}}{\alpha}, 1\right) R_{0i} \tag{46}$$

Due to the conversion of the phantom track speed range into a larger ECAV speed pseudo-range, the initial conditions of multiple ECAVs are constrained to stay within the original $r\dot{\theta}$-boundary range corresponding to their specified υ_E-range of $\pm 20\%$ for whatever value α actually is at any time instance (see figure 6 above). Therefore, equations (45) and (46) specify a maximum range, in which the selected initial condition values for each ECAV must also satisfy the following conditions, where I contains an ordered set of index numbers for each ECAV participating.

$$\begin{aligned} &\text{if} \quad && r_{0i} < \frac{\upsilon_{Emin}}{\alpha} R_{0i} \qquad \text{for any } i \in I \\ &\text{then} \quad && r_{0i} < \min_{j \in I}\left(\frac{r_{0j}}{R_{0j}}\right) \frac{\upsilon_{Emax}}{\upsilon_{Emin}} R_{0i} \quad \forall i \in I \end{aligned} \tag{47}$$

$$\begin{aligned} &\text{if} \quad && r_{0i} > \frac{\upsilon_{Emax}}{\alpha} R_{0i} \qquad \text{for any } i \in I \\ &\text{then} \quad && r_{0i} > \max_{j \in I}\left(\frac{r_{0j}}{R_{0j}}\right) \frac{\upsilon_{Emin}}{\upsilon_{Emax}} R_{0i} \quad \forall i \in I \end{aligned} \tag{48}$$

In addition to the range of valid initial conditions, the time-dependent upper and lower bounds on the flyable range of an individual i^{th} ECAV generating a straight or circular phantom track for some range of θ are given below, where $R_i(t)$ is dimensional.

$$(r_{min})_i(t) = \min\left(\frac{\upsilon_{Epsmin}}{\alpha} R_i(t), r_i^{A0}(t), r_i^{Af}(t)\right) \tag{49}$$

$$(r_{max})_i(t) = \min\left(\frac{\upsilon_{Epsmax}}{\alpha}, 1\right) R_i(t) \tag{50}$$

In equation (49), the solutions $r_i^{A0}(t)$ and $r_i^{Af}(t)$ are to equation (18) from ECAV system A, and both use υ_{Epsmin} for their constant speed. In addition, $r_i^{A0}(t)$ uses $(r_{0min})_i$ for its initial value—determined from equation (45); and $r_i^{Af}(t)$ uses $(r_{fmin})_i$ for its final value—determined from equation (45) with subscript f substituted for subscript 0. These special bounding solutions are represented graphically for specific cases in figures 7 through 9 as green ECAV trajectories. Equations (49) and (50) specify a maximum time-dependent flyable range, in which each ECAV's position must also satisfy conditions (47) and (48) for all time, with the following substitutions.

$$r_i(t) \rightarrow r_{0i}$$

$$R_i(t) \rightarrow R_{0i}$$

IX. Formulation of a Decentralized Cooperative Problem

As a first cut, the decentralized cooperative control problem—one of team coordination—is posed using the concept of coordination functions and the general bounds in (45)–(50); the aim here is to show one way the results from the previous section may be usefully applied to control the ECAV team. This problem is illustrated for a team of three ECAVs using mainlobe deception on three radars by creating a straight phantom track. To begin, assume a constant-course phantom track from right to left is desired, and that bounded ranges for υ_E, ϕ_E, and α have already been given as in (12). Let β be the absolute heading of the phantom track and n be the number of radars—equal to the number of ECAVs—then mathematically define the following parameters.

$$
\begin{aligned}
I &= [1, n] \in \mathbb{N} \\
i &= 1, 2, \ldots, n \\
rd_i &= (rd_{xi}, rd_{yi}) \in \mathbb{R}^2 \\
circle_i(x) &= rd_{yi} \pm \sqrt{(R_{max})_i{}^2 - (x - rd_{xi})^2} \\
cone_i &= \left(\beta + \frac{\pi}{2}\right) \pm \left(\frac{\pi}{2} - \phi_{Emin}\right)
\end{aligned}
$$

In the definitions above, the location of each radar is rd_i. The *circle* and *cone* equations represent subsets of the total space where deception is possible for each radar/ECAV pair given the radar's maximum operational range and the ECAV's course/antenna limitations from (12). With the above parameter definitions, the following function can be defined, which maps these parameters into the set of candidate functions that will later be used as inputs to each ECAV's coordination function.

$$
h_{\mathcal{T}}(rd_{i\in I}, (R_{max})_{i\in I}, \beta, \phi_{Emin}) \rightarrow \mathcal{T}_{\mathcal{B}}
$$

The set $\mathcal{T}_{\mathcal{B}}$ consists of all functions $f(x)$ specifying possible phantom tracks that all ECAVs can deceptively create for the participating radar network; thus, each function lies in the space $\mathcal{B}$—common to all *circle* and *cone* bounded areas. Mathematically, each function $f(x)$ satisfies the following conditions; the second condition is specific to the straight phantom track case.

$$
(x, f(x)) \in \left(\bigcap_{i\in I} circle_i\right) \bigcap \left(\bigcap_{i\in I} cone_i\right) =: \mathcal{B}
$$

$$
\frac{\mathrm{d}f}{\mathrm{d}x} \equiv \tan\beta
$$

Figure 10 below illustrates the mathematics introduced so far, where $n = 3$ radars. The blue lines represent functions in $\mathcal{T}_{\mathcal{B}}$ and are all possible candidates for the team-optimal phantom track, i.e. each may be generated given the three-radar situation and taking into account each radar's maximum range (gray solid lines) and the course/antenna bounds associated with the ECAVs (black dashed lines).

Three variables have yet to be chosen before a given phantom track is decided for the ECAV team. These variables and one approach to choosing them are given below.

$f(x)$ Let the phantom track as a function of x be determined by the cooperative control process.

x_0 For simplicity, assume that the longest length of phantom track is desirable, so choose x_0 by using the right-side boundary of $\mathcal{B}$, $x_0(y)$, and set $x_0(y) > x$ by the right-to-left assumption.

α Since the phantom target speed already has an allowable range of $\pm 20\%$, assume its nominal or mean value is fixed by the type of phantom target being created, but ensure $\alpha > 1.5$ to use the full ECAV speed and phantom target speed ranges.

Given the variables $f(x)$, x_0, and α, the following function may be defined, which uses these variables to determine valid initial condition bounds for each ECAV—using equations (45) and (46)—and/or time-dependent bounds for the flyable range of each ECAV—using equations (49) and (50).

$$
h_r(rd_i, f(x), x_0, \alpha) \rightarrow \begin{array}{l} [r_{0min}, r_{0max}]_i\,,\ \bar{\theta}_{0i} \\ [r_{min}(t), r_{max}(t)]_i\,,\ \theta_i(t) \end{array}
$$

The intermediate calculations needed for using equations (45) and (46) to find r_{0min} and r_{0max} for each ECAV are given below.

$$
\begin{aligned}
R_{0i} &= \|(x_0, f(x_0)) - rd_i\|_2 \\
\bar{\theta}_{0i} &= \arg(f(x_0) - rd_{yi}, x_0 - rd_{xi}) \\
\psi_i &= \bar{\theta}_{0i} - \arctan\frac{\mathrm{d}f}{\mathrm{d}x} \\
\dot{\theta}_{0i} &= \alpha \sin\psi_i
\end{aligned}
$$

The additional intermediate calculations needed for using equations (49) and (50) to find $r_{min}(t)$ and $r_{max}(t)$ for each ECAV are given below.

$$R_i(t) = R_{0i}\sqrt{1 + \alpha^2 t^2 - 2\alpha t \cos\psi_i}$$
$$\theta_i(t) = \arcsin\left(\frac{\alpha t \sin\psi_i}{R_i(t)}\right)$$
$$\dot{\theta}_i(t) = \frac{\alpha \sin\psi_i}{1 + \alpha^2 t^2 - 2\alpha t \cos\psi_i}$$

Of the seven intermediate equations listed above, the last five are specific to the straight phantom track case. Recall that conditions (47) and (48) must be applied to the choice of initial conditions and positions over time for each ECAV.

Two cost functions are now defined for each ECAV and for a given phantom track $f(x)$ as follows, where the cost could be figured based on a variety of factors such as fuel or radiated power required for deception.

$$icost_i([r_{0min}, r_{0max}]_i, \bar{\theta}_{0i})$$

$$tcost_i([r_{0min}, r_{0max}]_i, \bar{\theta}_{0i}, [r_{min}(t), r_{max}(t)]_i, \theta_i(t))$$

The initial cost of each ECAV, *icost*, measures how hard it would be for that ECAV to move from its current position to the initial position required for commencing a given phantom track. Note that the time-dependent cost of each ECAV, *tcost*, is not defined to depend on the positions of other ECAVs despite conditions (47) and (48); rather, the cost simply depends on the maximum flyable range of each ECAV before these conditions are applied to actual positions.

Finally, a cost based on the initial conditions and flyable ranges of each ECAV can be computed as a function of the track choice, $f(x)$—the only variable left to be chosen—which leads to the following coordination function for each ECAV with three variations possible.

$$h_i(f(x)) \rightarrow \begin{cases} icost_i \\ tcost_i(t) \\ icost_i + tcost_i(t) \end{cases}$$

Each ECAV passes only a coordination function, h_i, to the team leader. The team leader then uses all n coordination functions to find the function, $f(x)$, that will minimize the total cost of the team and specify the team-optimal phantom track for the ECAVs to create. If the first version of the coordination function is used, then each ECAV must know four things: its own radar's location and maximum range, its initial condition line $x_0(y)$, and the phantom track speed. If the second or third versions of the coordination function are used, then each ECAV must additionally know the locations and maximum ranges of all additional radars involved because its time-dependent flyable range depends on where the phantom track stops as well as starts. If the flyable ranges were defined to be only the space in between minimum and maximum pseudo-speed isolines (see figures 7 through 9), then the flyable range for each ECAV would only be a function of x and not t. Thus, each ECAV would only need to know its own radar's location and maximum range if version two of the coordination function above were used. Assuming that the third version of the coordination function is realistically most accurate, there is a tradeoff between the amount of information communicated to each ECAV and the accuracy of the team cost for generating a phantom track.

Figure 10 below illustrates the situation once the variables x_0 and α as well as $f(x)$ are chosen to specify a team-optimal phantom track as discussed above. The bold blue line represents the phantom track chosen optimally via the coordination functions $h_i(f(x))$, and the yellow lines represent the resulting range of valid initial conditions from which each corresponding ECAV may start at time zero. Time-dependent flyable ranges for each ECAV are not shown in the figure.

Besides using coordination functions, several other methods are available in treating the decentralized cooperative control problem. The common goal is to use the minimum amount of communication—or minimum amount of the team state information, such as ECAV positions—needed to achieve the desired level of performance in choosing a team-optimal phantom track.

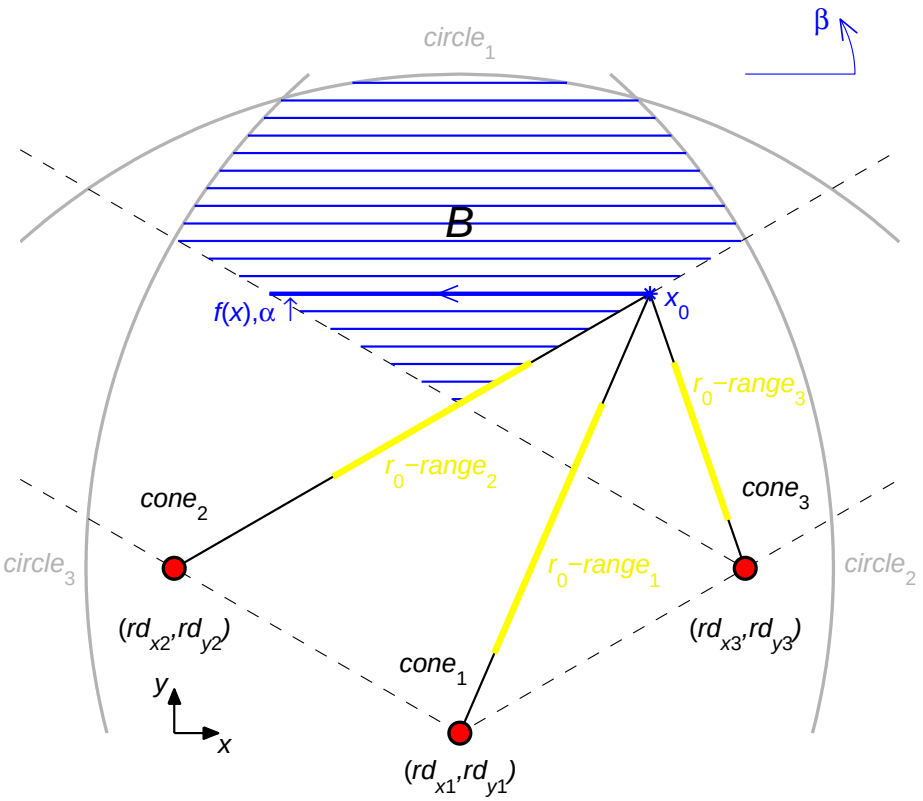

Figure 10. Decentralized Cooperative Control Problem for 3 radars and a straight phantom track.

X. Conclusion

THIS paper has shown that for mainlobe deception, assuming the ECAV and phantom track speeds to be constant severely limits the set of initial conditions yielding complete ECAV trajectories for a reasonable range of $\theta = 0$ to 90 degrees. Assuming ranges for the ECAV and phantom track speeds and including a course bound to account for the ECAV having fixed antennas yielded a more realistic flyable range for the ECAV. Flyable ranges with the above assumptions were thoroughly investigated, determined, and verified via extensive ODE simulations for a straight phantom track, a simple circular phantom track with radar placed at its center, and a general circular phantom track with radar placed arbitrarily. The approach developed and used to compute ECAV trajectories and bounds given a straight or circular phantom track is modular for n radars and n ECAVs. The ECAV trajectory solutions require specifying one ECAV variable as a function of time—whether it be speed, course, heading, turn rate, speed rate, or acceleration. The general bounds developed that define ECAV valid initial conditions and flyable ranges were shown to be independent of whether the phantom track is straight or circular; this result may be applicable to other types of phantom tracks. Based on these general bounds, a decentralized cooperative control problem was formulated under certain assumptions using coordination functions. In this scheme, communication of one coordination function per ECAV—providing its individual cost for generating different phantom tracks—allowed the ECAV team to determine the optimal phantom track resulting in the lowest team cost.

References

[1]Stimson, G. W., *Introduction to Airborne Radar*, SciTech Publishing, Raleigh, NC, 2nd ed., 1998.

[2]Pachter, M., Chandler, P. R., Purvis, K. B., Waun, S. D., and Larson, R. A., "Multiple Radar Phantom Tracks from Cooperating Vehicles Using Range-Delay Deception," *Proc. of the 4th International Conf. on Cooperative Control and Optimization*, Destin, FL, 2003.